ACS APPLIED MATERIALS & INTERFACES

RESEARCH ARTICLE

www.acsami.org

Facile Fabrication of Functionalized Graphene Sheets (FGS)/ZnO Nanocomposites with Photocatalytic Property

Yang Yang, Lulu Ren, Chao Zhang, Shu Huang, and Tianxi Liu*

Key Laboratory of Molecular Engineering of Polymers of Ministry of Education, Department of Macromolecular Science, Fudan University, Shanghai 200433, People's Republic of China

ABSTRACT: Functionalized graphene sheets (FGS)/ZnO nanocomposites were fabricated via thermal treatment method, using graphene oxide as a precursor of graphene, $Zn(NH_3)_4CO_3$ as a precursor of zinc oxide, and poly(vinyl pyrrolidone) as an intermediate to combine zinc with carbon materials. Thermogravimetric analysis, X-ray diffraction (XRD), Fourier transform infrared (FTIR) spectroscopy, transmission electron microscopy (TEM), and scanning electron microscopy (SEM) were used to characterize crystal structure and morphology of FGS/ZnO nanocomposites. It was shown that the well-dispersed ZnO nanoparticles were deposited on FGS homogeneously. The composites exhibited photocatalytic activity to decompose rhodamine 6G efficiently under low-power ultraviolet (UV) light. This facile and low-cost method makes the composite a perfect candidate in applications of catalysis and other areas.

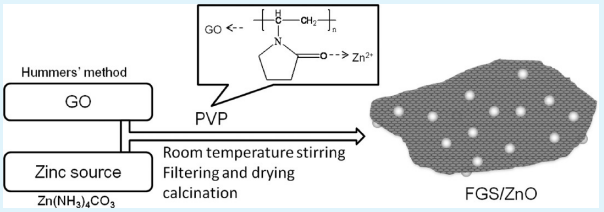

KEYWORDS: graphene, ZnO, nanocomposites, photocatalytic property

INTRODUCTION

Graphene, as a single-layer one-atom-thick graphitic carbon material, has recently attracted intense scientific interest, because of its large surface area and extraordinary electrical, thermal, and mechanical properties.[1−3] One of the most promising and scalable approaches to obtain graphene is to convert graphene oxide, generated by the oxidization and subsequent exfoliation of graphite, to graphene via chemical reduction or thermal treatment.[3−5] However, because of the van der Waals interactions between monolayer graphene sheets, which lead to an irreversibly restacking tendency during the reduction process, it is preferred to obtain few layers graphene rather than single-layer graphene. The restacked structure would lead to a dramatic decrease of specific surface area of graphene, which is unfavorable for wide applications of graphene. Many methods have been developed to solve this problem such as using surfactant to stabilize graphene nanosheets, grafting polymer chains to change the polarity of graphene surface, and decorating graphene surface with metal or semiconductor inorganic nanoparticles to decrease the π-stacking interactions between graphene sheets.[6−12]

As a promising semiconductor material, ZnO has received great attention, because of its wide band gap (3.37 eV) and large exaction binding energy (60 meV). It has broad technological applications such as photonic crystals, catalysts, light-emitting diodes, sensors, and electroluminescent and photoluminescent materials.[13] Hybridization of carbon materials with ZnO offers a powerful way to obtain many interesting properties such as ultrafast nonlinear optical switching properties,[14] optoelectronic properties,[15−17] energy storage properties,[18] and photocatalytic activity.[19,20] Various methods such as thermal decomposition,[14,21,22] covalent coupling,[15] electrochemical route,[16] noncovalent modification,[20] and sol−gel process[23] have been employed to obtain these composites and explore their renewed properties.

Williams et al.[24] mixed ZnO nanoparticles and graphene oxide (GO) sheets in ethanol and investigated the excited-state interactions between ZnO nanoparticles and GO. The electron transfer from excited ZnO nanoparticles to GO can be effective in carrying out the reduction of GO and decreasing the resistivity of the reduced graphene. Zheng et al.[25] reported that graphene sheets with pyramid-like morphologies have been grown on the ZnO nanowires coated with Ni catalyst nanoparticles by plasma-enhanced chemical vapor deposition (PECVD), and a greatly improved field-emission (FE) property for the hybrid ZnO/graphene sheets material has been achieved. This overcame the FE problem of graphene. Wu et al.[26] presented a general approach for the preparation of sandwich-like graphene/ZnO nanocomposites by solvothermal method in ethylene glycol medium. The decorated ZnO nanoparticles can effectively prevent the graphene sheets from stacking together. The sandwich-like structure can not only improve the ultraviolet−visible (UV−vis) absorption of ZnO, but also enhance the thermal stability of graphene. Kim and co-workers[27,28] reported the vertical growth of ZnO nanostructures on graphene layers using catalyst-free metal−organic vapor-phase epitaxy (MOVPE) and demonstrated a novel transparent and flexible optoelectronic hybrid material. Because of the good mechanical and electrical contact between vertical ZnO nanowires and graphene, the FE of the hybrid material showed low turn-on voltages. Lee et al.[29] fabricated ZnO nanorod-graphene by metal−organic chemical

Received: May 5, 2011
Accepted: June 17, 2011
Published: June 17, 2011

vapor deposition (MOCVD) for multifunctional conductors, and the ZnO/graphene composites showed good electrical conductance and good optical transparency, comparable to that of a homogeneous graphene layer, as well as UV and visible-light emissions inherited from the ZnO nanorods. Zhang et al.[30] deposited ZnO on graphene by ultrasonic spray pyrolysis and the graphene−ZnO composite film exhibited an enhanced capacitive behavior with better reversible charging/discharging ability and high capacitance values. Besides all the applications mentioned above, such carbon material/ZnO systems also exhibit excellent capacity in photocatalysis, because ZnO is a good electron donor with high optical activity and stability, high sensitivity for UV−vis light and low fabrication cost and graphene is an excellent electron acceptor; thus, the hybrid systems can act in a cooperative way by increasing migration efficiency of photoinduced electrons and effectively reduce recombination and improve photocatalytic activity.[26,31,32]

Therefore, fabricating graphene/ZnO composites with high photocatalytic efficiency via a facile and low-cost method is crucial for applications related with several environmental issues. However, the fabrication methods mentioned above have their limits. For the simple mixing method, because of the weak interaction between ZnO and graphene, the loading capacity of ZnO onto graphene is limited.[24] Meanwhile, fabrication methods using chemical vapor deposition (CVD), vapor-phase epitaxy (VPE), ultrasonic spray pyrolysis, et al. require special equipment.[25−30] In this article, we reported a facile method to fabricate a hybrid structure by anchoring ZnO nanoparticles on functionalized graphene sheets (FGS), using poly(vinyl pyrrolidone) (PVP) as an intermediate to combine zinc ions with carbon materials and investigated its photocatalytic property. Water-soluble $Zn(NH_3)_4CO_3$ and monodispersed GO were used as precursors of ZnO nanoparticles and FGS, respectively, and the transformations occurred during thermal treatment. This method is supposed to be easily amplified at low cost, because (i) the raw materials are inexpensive, (ii) the fabrication process is simple, and (iii) the necessary pieces of equipment, such as a stirrer, a dryer, a filter, and a calcining furnace are common. The as-prepared composite with ZnO nanoparticles monodispersed on graphene sheets exhibits photocatalytic activity.

EXPERIMENTAL METHODS

Materials. Natural graphite powder (325 mesh) was commercially obtained from Alfa-Aesar. PVP (molecular weight of M_w = 85 000−124 000) was purchased from Sigma−Aldrich. In addition, 37% hydrochloric acid (HCl), 98% sulfuric acid (H_2SO_4), 30% hydrogen peroxide (H_2O_2), potassium manganese oxide ($KMnO_4$), sodium nitrate ($NaNO_3$), $Zn(NO_3)_2 \cdot 6H_2O$, $(NH_4)_2CO_3$, and ammonia were supplied by China Medicine Co. All reactants were of analytical purity and used as received.

Preparation of Graphite Oxide. Graphite oxide was produced using a modified Hummers' method from graphite powder.[33] In detail, 2 g of graphite powder and 1 g of $NaNO_3$ in 50 mL of concentrated H_2SO_4 were vigorously stirred in an ice bath. Six grams (6 g) of $KMnO_4$ was added gradually with stirring, to prevent the temperature of the mixture from exceeding 10 °C. The ice bath was then removed and the mixture was stirred at 35 ± 3 °C for 30 min. Upon completion of the reaction, 92 mL of distilled water was added, and the temperature was kept at 98 °C for 15 min. The reaction was terminated by adding 280 mL of distilled water and 30 mL of 30% H_2O_2 solution. The mixture was filtered, and washed successively with 5% HCl aqueous solution completely until sulfate could not be detected with $BaCl_2$. Finally, graphite oxide was obtained after drying under vacuum at 50 °C for 24 h.

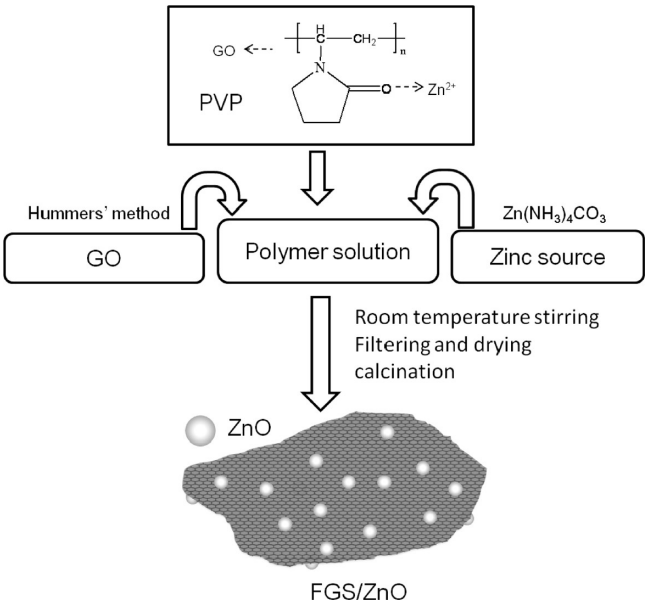

Figure 1. Schematic of the fabrication process for FGS/ZnO nanocomposites.

Fabrication of Functionalized Graphene Sheets (FGS)/ZnO Nanocomposites. Water-soluble $Zn(NH_3)_4CO_3$ solution was prepared by mixing 25 mL of $Zn(NO_3)_2$ (0.25 M) aqueous solution, 23 mL of $(NH_4)_2CO_3$ (0.26 M) aqueous solution, and 2 mL of ammonia to form solution A. Graphite oxide (0.1 g) was ultrasonicated in deionized water with 0.1 g of PVP to form a GO solution (solution B). The two solutions were mixed and stirred at room temperature for 2 h, then filtered and washed with deionized water to remove the free Zn^{2+} ions. Finally, the sample was dried at 80 °C overnight to obtain the dried precursor of FGS/ZnO, and then further calcinated at 300 °C for 3 min under an environmental atmosphere to obtain FGS/ZnO nanocomposites. A schematic of the fabrication of FGS/ZnO nanocomposites is shown in Figure 1. Samples without GO or PVP were also fabricated using a similar procedure, for comparison. The samples were calcinated to constant weight under air conditions to remove FGS and PVP; the residual weight ratios of the samples was considered to be the ZnO content. The ZnO content of FGS/ZnO and FGS/ZnO without PVP were estimated to be 39.8% and 21.5%, respectively.

CHARACTERIZATIONS

Thermogravimetric analysis (TGA) was performed under nitrogen flow from 50 °C to 800 °C using a Pyris 1 TGA apparatus. FTIR spectra over the range of 4000−400 cm^{-1} were recorded on a NEXUS-470 spectrometer, using KBr pellets. X-ray diffraction (XRD) patterns were recorded with a Bruker GADDS X-ray diffractometer that was using Cu Kα radiation under a voltage of 40 kV and a current of 40 mA. Transmission electron microscopy (TEM) (Philips, Model CM 300 FEG), scanning electron microscopy (SEM) (Vega Model TS 5136MM), and atomic force microscopy (AFM) (NanoScope IV) were used to observe the morphology of the samples. Photocatalytic experiments

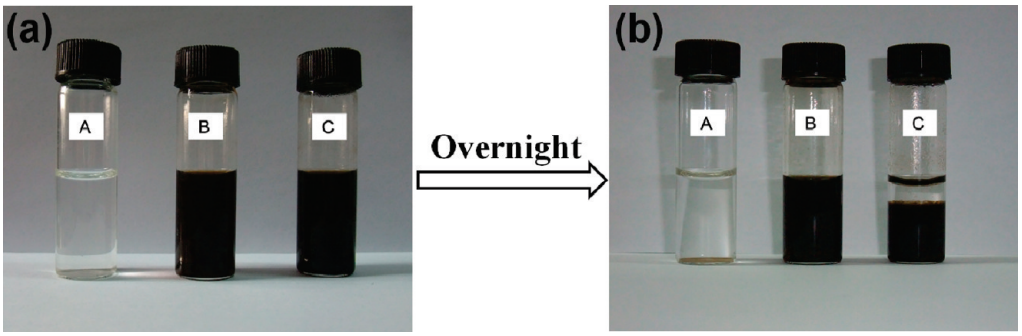

Figure 2. Digital photos of (a) as-prepared and (b) overnight solutions of A precursor (ZnO), B precursor (FGS/ZnO), and C precursor (FGS/ZnO without PVP).

were carried out by adding 10 mg FGS/ZnO nanocomposites into 200 mL of 10 mg L^{-1} rhodamine 6G (Rh6G). The suspensions were illuminated using a 100-W high-pressure mercury lamp. The UV−vis spectra were performed on a Shimadzu Model UV-1601 spectrophotometer.

RESULTS AND DISCUSSION

Compared with graphene, GO sheets can be dispersed well in water and, thus, can form a stable colloidal suspension. It is widely accepted that hydrophilicity caused by oxygen functional groups,[34] repulsive force caused by negative charge on sheets, and wrinkles of the sheets[35] contribute much to the stability. Therefore, adding $Zn(NH_3)_4CO_3$ into GO solution changed the charge density of GO sheets, and destroyed the stability of GO colloid, thus leading to agglomerations and the agglomerations gradually deposited to the bottom of the vial, as shown in Figure 2C. PVP, which is a water-soluble linear polymer, is effective on solubilization of CNT and graphene in water by wrapping and hydrophobic interaction between sp^2-carbon conjugate structures and PVP chains.[36,37] Moreover, PVP is also an intermedium depositing nanoparticles onto carbon materials[22,38] and a directing reagent developed to control the morphology and promote crystallization of ZnO.[39] Therefore, PVP has been used as an additive to stabilize GO sheets, promote the formation of ZnO particles, and deposit them onto the carbon sheets. Figure 2 shows the digital photos of as-prepared and overnight solution of precursor A (ZnO), B (FGS/ZnO), and C (FGS/ZnO without PVP). The solution of precursor of ZnO is transparent and nothing can be collected by the filter, because the precursor of ZnO has good solubility in water. The solutions of precursors of FGS/ZnO with and without PVP appear brown in color, because of the existence of GO. The precursor of FGS/ZnO without PVP precipitated from the solution after 24 h, whereas the FGS/ZnO precursor with PVP dispersed well with no sign of aggregation. PVP greatly stabilizes GO sheets and maintains their good dispersion with the existence of $Zn(NH_3)_4CO_3$.

After collecting the precursor of FGS/ZnO from the solution by filtering, the FGS/ZnO nanocomposites was obtained by drying and calcining. The thermal treatment process is very important for the formation of FGS/ZnO, because ZnO nanoparticles can be obtained by thermal decomposition of ZnO precursor and the dried GO also needs thermal exfoliation to give rise to FGS.[40,41] Since both of the transformations are accompanied with weight loss, we can use TGA to investigate the converting process. TGA curves of graphite oxide, PVP, and the dried precursor of FGS/ZnO are shown in Figure 3. Graphite

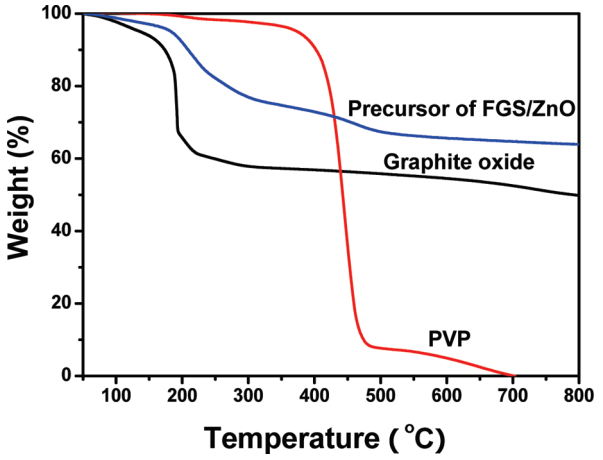

Figure 3. TGA curves of graphite oxide, PVP, and a FGS/ZnO precursor.

oxide shows a significant weight loss at ~200 °C and PVP shows good thermal stability until 400 °C. For FGS/ZnO, the TGA curve exhibits two main weight loss steps: the first stage, in the range of 200−300 °C, is consistent with the ZnO formation process from $Zn(NH_3)_4CO_3$ decomposition, as reported previously;[42] the second step, in the range of 400−500 °C, corresponds to the decomposition of PVP. However, the weight loss caused by GO in the as-prepared FGS/ZnO could not be identified in this curve. This is due to the thermal shielding effect caused by the existence of PVP, and the weight loss of GO is delayed and overlapped with the formation process of ZnO.

FTIR spectra of graphite oxide, FGS and FGS/ZnO nanocomposites, and FGS/ZnO without PVP are shown in Figure 4. For graphite oxide, the peaks at 3450, 1740, 1630, 1400, and 1100 cm^{-1} are assigned to the −OH stretching vibrations, C═O stretching vibrations in carboxylic acid, skeletal vibrations of unoxidized graphitic domains, O−H deformations of the C−OH groups, and C−O stretching vibrations, respectively.[1] Compared to graphite oxide, the spectrum of FGS shows the absence of the characteristic peaks of carboxyl group at 1740 cm^{-1} and hydroxide group at 1400 cm^{-1}, while the other bands remained unvaried, indicating that the GO has been partially deoxygenated during the calcination process. For FGS/ZnO without PVP, the spectrum is similar to that of FGS and the absorption peak belonging to the Zn−O vibration that is supposed to appear at 460 cm^{-1} is barely identified. This may be due to the low content and poor crystallinity of ZnO in this

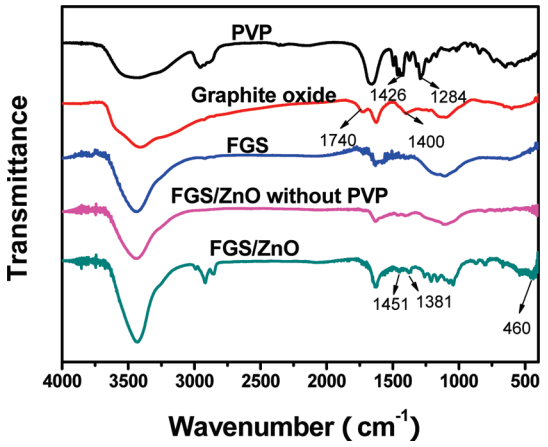

Figure 4. Fourier transform infrared (FTIR) spectra of graphite oxide and FGS and FGS/ZnO nanocomposites.

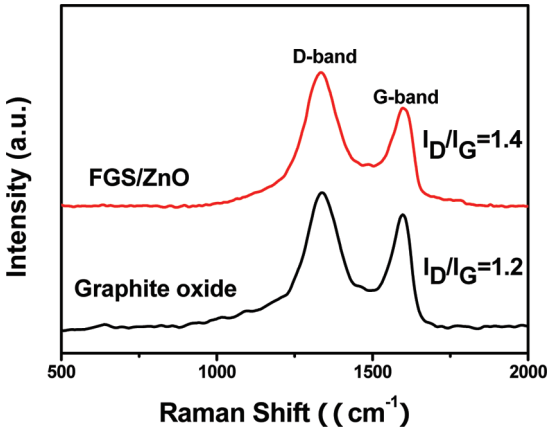

Figure 5. Raman spectra of graphite oxide and FGS/ZnO nanocomposites.

sample. In the spectrum of FGS/ZnO, we can observe the typical peaks belonging to FGS, a new broad peak at 460 cm^{-1} identified to the vibration of Zn−O belonging to ZnO nanoparticles, and several characteristic bands of PVP: the alkyl C−H stretching vibration between 2950 and 2850 cm^{-1}, and N→H−O complex and the pyrrolidone-ring-related bonds at 1381 and 1451 cm^{-1}, respectively. For pure PVP, N→H−O complex and the pyrrolidone-ring-related bonds display characteristic absorptions at 1284 and 1426 cm^{-1}, respectively. The large shifts can be ascribed to an interaction between the O and N atoms of the pyrrolidone ring and the specific ZnO crystallographic plane.[39]

Raman spectra of GO and FGS/ZnO are shown in Figure 5. The D/G intensity ratio (where the D peak is a defect peak due to intervallic scattering and G refers to the graphene G peak) of FGS/ZnO increases, compared with that of the GO. The increase of D/G intensity ratio indicated an increase in the number of smaller sp^2 domains, which is usually observed in the Raman spectra of reduced GO,[43] indicating the successful transformation from GO to FGS.

The crystal structure and particle size distribution of FGS/ZnO nanocomposites were characterized by XRD. The XRD patterns of graphite oxide and FGS/ZnO fabricated without PVP were also recorded for comparison (see Figure 6). GO has a diffraction peak centered at $2\theta = 10.0°$, corresponding to a (002) interplanar spacing of 8.8 Å. However, this peak disappears for

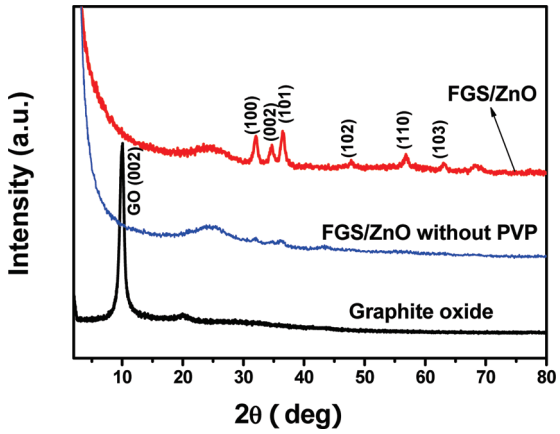

Figure 6. XRD patterns of graphite oxide, FGS/ZnO nanocomposites, and FGS/ZnO without PVP.

FGS/ZnO nanocomposites and a new broad peak at 2θ = 20°−30° appears, indicating the disordered stacking of graphene sheets in the composites.[44,45] Moreover, a typical pattern of ZnO with hexagonal structure (JCPDS No. 36-1451) is identified in this curve of FGS/ZnO nanocomposites. The mean particle size of ZnO nanoparticles can be estimated via the Scherrer equation, using the full width at half-maximum (fwhm) of the peaks belonging to ZnO and is calculated to be ∼7.8 nm. Whereas the pattern of ZnO is hardly identified in the curve of FGS/ZnO nanocomposite fabricated without PVP (the blue curve). The extremely weak intensity of ZnO in this curve can be ascribed to its poor crystallinity or low content or both. Because the ZnO content decreases from 39.8% to 21.5% would not be able to lead to such a dramatic decrease of the intensity, the poor crystallinity plays the major role. PVP used here can not only increase the retaining amount of Zn^{2+} ions in filtration by connecting the ions with GO sheets, but also promote ZnO nucleation and crystal growth by coordinating the water from the dehydration reaction of the ZnO precursor, because of the decreased diffusion of Zn^{2+} ions into water caused by the increased viscosity and the interaction between PVP and Zn^{2+} ions.

To further characterize the morphology of the FGS/ZnO hybrid, TEM observations were conducted. Samples were prepared by dipping holey carbon mesh grids into the ultrasonicated suspension and drying them in air. From the TEM image of GO (see Figure 7a), thin sheets larger than several micrometers with wrinkles were observed.[46,47] The contrast of GO sheets is very low, because of the thin thickness of the sheets. The AFM image of GO shown in the inset of Figure 7a exhibits that GO sheets are approximately several micrometers large with irregular shapes. In addition, the thickness of GO sheets is ∼0.7 nm, indicating a full exfoliation of graphite oxide. Typical TEM images of FGS/ZnO (see Figures 6b and 6c) at different magnifications show that the composites consisted of two-dimensional FGS decorated with ZnO nanoparticles. ZnO nanoparticles are well-separated from each other and well spread out on the FGS. Meanwhile, the disappearance of wrinkles may be attributed to the dense decoration of ZnO, which was also reported in a graphene−CdS hybrid.[48] ZnO nanoparticles deposited on the FGS were quasi-spherical in shape and had a uniform particle size of ∼7 nm, which is much smaller than the ZnO particles (usually dozens of nanometers) obtained by thermal decomposition.[42] The lattice fringes belonging to hexagonal ZnO crystals can be identified in

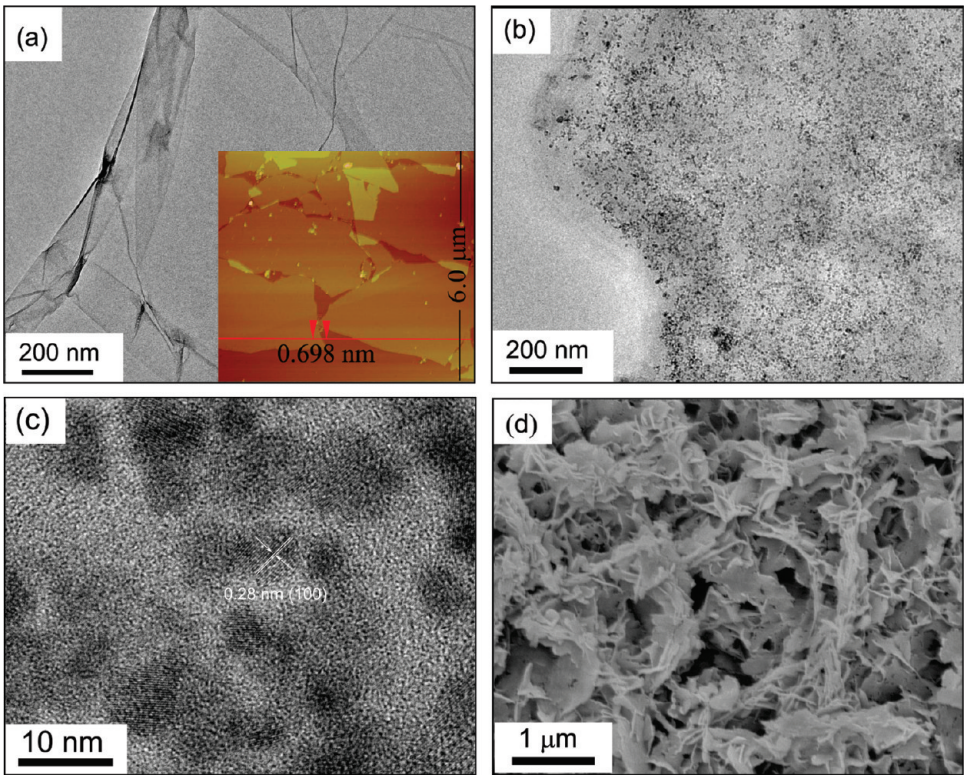

Figure 7. (a) Transmission electron microscopy (TEM) image of GO sheets (inset shows the atomic force microscopy (AFM) image of GO sheets); (b) low-magnification TEM image; (c) high-magnification TEM image; and (d) low-magnification scanning electron microscopy (SEM) image of FGS/ZnO nanocomposites.

Figure 7c, and the disordered stacking of FGS/ZnO nanocomposites shown in Figure 7d is consistent with the diffusing halo at $2\theta = 20°-30°$ in the XRD pattern for FGS/ZnO nanocomposites (see Figure 6). We can also estimate the size of FGS/ZnO sheets by measuring the edge length of composite sheets in Figure 7d. The sheet size of FGS/ZnO is ~1 μm, on average, and is smaller than that of the GO sheets that we observed from the AFM image. This is because GO sheets would be broken into smaller pieces during calcination. However, the size of graphene does not show great influence on the structure and properties of the composite (except for the sheets size), because these smaller graphene sheets still have an extremely large radius−thickness ratio and a much larger surface, compared to the diameter of the ZnO particle.

Therefore, we successfully fabricated FGS/ZnO nanocomposites with small ZnO attached onto FGS. Chen et al.[49] fabricated two types of ZnO/reduced graphite oxide (with dense and exfoliated graphite oxide) composites, using $ZnSO_4$ and graphite oxide as precursors under basic conditions and the ZnO size calculated from XRD is ~25 nm. Guo et al.[38] fabricated multiwalled carbon nanotube (MWCNT)/ZnO nanoparticles composite using a similar method, but they evaporated the mixture of $Zn(NH_3)_4CO_3$, MWCNT, and PVP until dry. Most of ZnO particles are ~10 nm in size, but some much bigger particles (as large as >100 nm) also can be observed. In our fabrication, the precursor solution of FGS/ZnO was filtered, and because the precursor of ZnO was water-soluble, the free precursor of ZnO, which was not attached to GO, will flow away with the filtrate. Therefore, it is more likely that only the supported ZnO precursor has the chance to be transformed to ZnO nanoparticles.

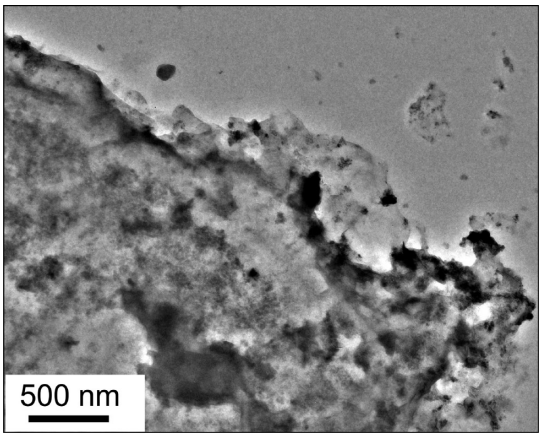

Figure 8. TEM image of the FGS/ZnO nanocomposites treated with ultrasonication and stir.

Therefore, the introduction of PVP, the water-soluble precursor, and the allowed loss of free precursor in filter process play important roles to obtain uniform and small ZnO particles, which are attached to FGS.

The sample was ultrasonicated for 30 min, followed by stirring for 2 h, to examine the stability of the heterostructure of FGS/ZnO nanocomposites, and the TEM image is shown in Figure 8. Although a few particles and some small pieces that are supposed to be the ZnO particles falling off from FGS sheets and the fragments broken-off from the composite sheets, respectively, most of the composite maintains its original morphology with

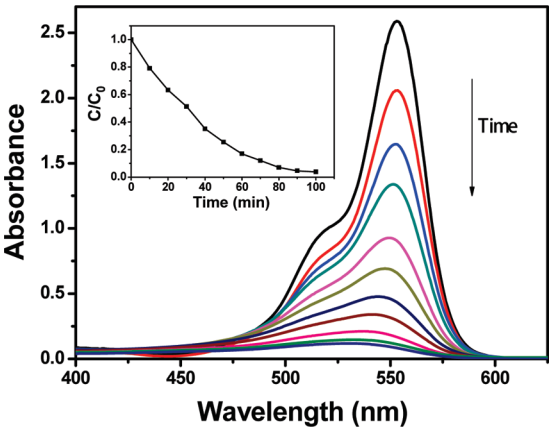

Figure 9. UV−vis absorption spectra of the rhodamine solution during the photodegradation. The inset shows the decomposition of the rhodamine solution using FGS/ZnO nanocomposites.

ZnO nanoparticles attached on FGS sheets. It is well-known that the valence band electrons of ZnO can be excited to its conduction bands, giving rise to the formation of high-energy electron−hole pairs, when they are irradiated by UV light, the photocatalytic activity of ZnO particles depends on the synthesis method, morphology, crystallinity, and surface properties.[50−52] The combination of ZnO particles with carbon materials can increase the energy levels of the conduction and valence band edges, which would improve the redox potentials to utilize UV light in photocatalysis.[53] The photocatalytic activity of the FGS/ZnO nanocomposites that we fabricated in this article is examined. Rh6G solutions exposed under UV light in the presence of FGS/ZnO were taken out at regular time intervals and their UV−vis absorption spectra are shown in Figure 9. The absorption of these solutions decreased gradually with irradiation time, and the variation of Rh6G concentration calculated using the maximum absorption of the solution is shown in the inset. After exposure under UV light for 30 min, 50% Rh6G was degraded and the decomposition efficiency increases to 96% after 100 min. The photocatalytic activity of pure ZnO particles, which is the same as that in the composite, was not examined for comparison, because the ZnO precursor is water-soluble and nothing remains during the filtration process. Chen et al.[49] reported that the decomposition efficiency of the two types of ZnO/reduced graphite oxide (with dense and exfoliated graphite oxide) and pure ZnO were 50.2%, 70.3%, and 28.0%, respectively, after decomposition under UV light for 30 min, by dispersing 0.05 g of sample in 50 mL of aqueous methyl orange solution under a 250-W high-pressure mercury lamp. The composite exhibits an enhancement of photocatalytic activity, compared to ZnO, because of the interaction between ZnO and carbon materials. Considering the experimental conditions (10 mg of sample in 200 mL of solution under a 100-W high-pressure mercury lamp), the efficiency of our sample shows great improvement, compared to that of pure ZnO, and is comparable to that of ZnO/reduced graphite oxide. Therefore, we believe that the high photocatalytic activity of our sample also benefits significantly from the introduction of FGS. Based on the literature, we believe that the increased photon absorbance caused by FGS and electron transfer between ZnO with good crystallinity and FGS contribute significantly to the high decomposition efficiency.[19,23,50]

CONCLUSIONS

A simple, effective, and scalable method was developed to fabricate functional graphene sheets (FGS)/ZnO nanocomposites. Well-dispersed ZnO nanoparticles with an average diameter of 7 nm were deposited on FGS homogeneously via the thermal decomposition of a mixture of $Zn(NH_3)_4CO_3$, graphene oxide (GO), and poly(vinyl pyrrolidone) (PVP). The PVP component plays an indispensable role for loading ZnO nanoparticles onto FGS by connecting Zn ions on the carbon materials and promoting ZnO nucleation and crystal growth in the precursor-prepared process. The FGS/ZnO nanocomposites thus prepared exhibit photocatalytic activity, and the facile and low-cost method makes the composite a perfect candidate to be used for a variety of environmental issues.

AUTHOR INFORMATION

Corresponding Author
*E-mail: txliu@fudan.edu.cn.

ACKNOWLEDGMENT

We gratefully acknowledge financial support from the "Shu Guang" project (No. 09SG02), supported by Shanghai Municipal Education Commission and Shanghai Education Development Foundation.

REFERENCES

(1) Guo, H.-L.; Wang, X.-F.; Qian, Q.-Y.; Wang, F.-B.; Xia, X.-H. *ACS Nano* **2009**, *3* (9), 2653–2659.
(2) Zhou, Y.; Bao, Q.; Tang, L. A. L.; Zhong, Y.; Loh, K. P. *Chem. Mater.* **2009**, *21* (13), 2950–2956.
(3) Li, D.; Muller, M. B.; Gilje, S.; Kaner, R. B.; Wallace, G. G. *Nature Nanotechnol.* **2008**, *3* (2), 101–105.
(4) Tung, V. C.; Allen, M. J.; Yang, Y.; Kaner, R. B. *Nature Nanotechnol.* **2008**, *4* (1), 25–29.
(5) Schniepp, H. C.; Li, J. L.; McAllister, M. J.; Sai, H.; Herrera-Alonso, M.; Adamson, D. H.; Prud'homme, R. K.; Car, R.; Saville, D. A.; Aksay, I. A. *J. Phys. Chem. B* **2006**, *110* (17), 8535–8539.
(6) Spitalsky, Z.; Danko, M.; Mosnacek, J. *Curr. Org. Chem.* **2011**, *15* (8), 1133–1150.
(7) Tummala, N. R.; Grady, B. P.; Striolo, A. *Phys. Chem. Chem. Phys.* **2010**, *12* (40), 13137–13143.
(8) Fang, M.; Wang, K. G.; Lu, H. B.; Yang, Y. L.; Nutt, S. *J. Mater. Chem.* **2010**, *20* (10), 1982–1992.
(9) Cao, Y. W.; Feng, J. C.; Wu, P. Y. *Carbon* **2010**, *48* (5), 1683–1685.
(10) He, H.; Gao, C. *Chem. Mater.* **2010**, *22* (17), 5054–5064.
(11) Zhang, H.-B.; Yan, Q.; Zheng, W.-G.; He, Z.; Yu, Z.-Z. *Appl. Mater. Interfaces* **2011**, *3* (3), 918–924.
(12) He, H.; Gao, C. *Appl. Mater. Interfaces* **2010**, *2* (11), 3201–3210.
(13) Pearton, S. J.; Norton, D. P.; Ip, K.; Heo, Y. W.; Steiner, T. *Prog. Mater. Sci.* **2005**, *50* (3), 293–340.
(14) Zhu, Y. W.; Elim, H. I.; Foo, Y. L.; Yu, T.; Liu, Y. J.; Ji, W.; Lee, J. Y.; Shen, Z. X.; Wee, A. T. S.; Thong, J. T. L.; Sow, C. H. *Adv. Mater.* **2006**, *18* (5), 587–592.
(15) Zhang, N.; Sun, J.; Jiang, D. Y.; Feng, T.; Li, Q. *Carbon* **2009**, *47* (5), 1214–1219.
(16) Zhang, R. X.; Fan, L. Z.; Fang, Y. P.; Yang, S. H. *J. Mater. Chem.* **2008**, *18* (41), 4964–4970.
(17) Liu, J. W.; Li, X. J.; Dai, L. M. *Adv. Mater.* **2006**, *18* (13), 1740–1744.
(18) Liu, J. P.; Li, Y. Y.; Ding, R. M.; Jiang, J.; Hu, Y. Y.; Ji, X. X.; Chi, Q. B.; Zhu, Z. H.; Huang, X. T. *J. Phys. Chem. C* **2009**, *113* (13), 5336–5339.

(19) Guo, Y.; Wang, H.; He, C.; Qiu, L.; Cao, X. *Langmuir* **2009**, *25* (8), 4678–4684.
(20) Jiang, L. Q.; Gao, L. *Mater. Chem. Phys.* **2005**, *91* (2−3), 313–316.
(21) Li, C. S.; Qiao, Y. J.; Li, Y. N.; Wu, Y. L. *Sci. China Ser. E* **2009**, *52* (5), 1254–1257.
(22) Guo, G.; Guo, J.; Tao, D.; Choy, W. C. H.; Zhao, L.; Qian, W.; Wang, Z. *Appl. Phys. A—Mater.* **2007**, *89* (2), 525–528.
(23) Zhu, L. P.; Liao, G. H.; Huang, W. Y.; Ma, L. L.; Yang, Y.; Yu, Y.; Fu, S. Y. *Mater. Sci. Eng. B* **2009**, *163* (3), 194–198.
(24) Williams, G.; Kamat, P. V. *Langmuir* **2009**, *25* (24), 13869–13873.
(25) Zheng, W. T.; Ho, Y. M.; Tian, H. W.; Wen, M.; Qi, J. L.; Li, Y. A. *J. Phys. Chem. C* **2009**, *113* (21), 9164–9168.
(26) Wu, J. L.; Shen, X. P.; Jiang, L.; Wang, K.; Chen, K. M. *Appl. Surf. Sci.* **2010**, *256* (9), 2826–2830.
(27) Kim, Y. J.; Lee, J. H.; Yi, G. C. *Appl. Phys. Lett.* **2009**, *95* (21), 13101–13101.
(28) Hwang, J. O.; Lee, D. H.; Kim, J. Y.; Han, T. H.; Kim, B. H.; Park, M.; No, K.; Kim, S. O. *J. Mater. Chem.* **2010**, *21* (10), 3432–3437.
(29) Lee, J. M.; Pyun, Y. B.; Yi, J.; Choung, J. W.; Park, W. I. *J. Phys. Chem. C* **2009**, *113* (44), 19134–19138.
(30) Zhang, Y. P.; Li, H. B.; Pan, L. K.; Lu, T.; Sun, Z. *J. Electroanal. Chem.* **2009**, *634* (1), 68–71.
(31) Li, B. J.; Cao, H. Q. *J. Mater. Chem.* **2011**, *21* (10), 3346–3349.
(32) Xu, T. G.; Zhang, L. W.; Cheng, H. Y.; Zhu, Y. F. *Appl. Catal., B* **2011**, *101* (3−4), 382–387.
(33) Hummers, W. S. J.; Offeman, R. E. *J. Am. Chem. Soc.* **1958**, *80* (6), 1339–1339.
(34) Kim, J.; Cote, L. J.; Kim, F.; Yuan, W.; Shull, K. R.; Huang, J. X. *J. Am. Chem. Soc.* **2010**, *132* (23), 8180–8186.
(35) Meyer, J. C.; Geim, A. K.; Katsnelson, M. I.; Novoselov, K. S.; Booth, T. J.; Roth, S. *Nature* **2007**, *446* (7131), 60–63.
(36) Hua, J.; Wang, Z.; Zhao, J.; Zhang, J.; Li, R.; Nie, H.; Sun, X. *Colloid Polym. Sci.* **2011**, 1–7.
(37) Yoon, S.; In, I. *J. Mater. Sci.* **2011**, *46* (5), 1316–1321.
(38) Gao, Y.; Jiang, P.; Liu, D. F.; Yuan, H. J.; Yan, X. Q.; Zhou, Z. P.; Wang, J. X.; Song, L.; Liu, L. F.; Zhou, W. Y.; Wang, G.; Wang, C. Y.; Xie, S. S.; Zhang, J. M.; Shen, D. Y. *J. Phys. Chem. B* **2004**, *108* (34), 12877–12881.
(39) Zhang, J. H.; Liu, H. Y.; Wang, Z. L.; Ming, N. B.; Li, Z. R.; Biris, A. S. *Adv. Funct. Mater.* **2007**, *17* (18), 3897–3905.
(40) Verdejo, R.; Barroso-Bujans, F.; Rodriguez-Perez, M. A.; de Saja, J. A.; Lopez-Manchado, M. A. *J. Mater. Chem.* **2008**, *18* (19), 2221–2226.
(41) Bon, S. B.; Valentini, L.; Verdejo, R.; Fierro, J. L. G.; Peponi, L.; Lopez-Manchado, M. A.; Kenny, J. M. *Chem. Mater.* **2009**, *21* (14), 3433–3438.
(42) Chen, C.; Liu, P.; Lu, C. *Chem. Eng. J.* **2008**, *144* (3), 509–513.
(43) Kudin, K. N.; Ozbas, B.; Schniepp, H. C.; Prud'homme, R. K.; Aksay, I. A.; Car, R. *Nano Lett.* **2007**, *8* (1), 36–41.
(44) Falcao, E. H. L.; Blair, R. G.; Mack, J. J.; Viculis, L. M.; Kwon, C. W.; Bendikov, M.; Kaner, R. B.; Dunn, B. S.; Wudl, F. *Carbon* **2007**, *45* (6), 1367–1369.
(45) Huai-Ping, C.; Jia-Jun, H.; Yang, L.; Shu-Hong, Y. *Small* **2010**, *6* (2), 169–173.
(46) Schniepp, H. C.; Li, J.-L.; McAllister, M. J.; Sai, H.; Herrera-Alonso, M.; Adamson, D. H.; Prud'homme, R. K.; Car, R.; Saville, D. A.; Aksay, I. A. *J. Phys. Chem. B* **2006**, *110* (17), 8535–8539.
(47) McAllister, M. J.; Li, J.-L.; Adamson, D. H.; Schniepp, H. C.; Abdala, A. A.; Liu, J.; Herrera-Alonso, M.; Milius, D. L.; Car, R.; Prud'homme, R. K.; Aksay, I. A. *Chem. Mater.* **2007**, *19* (18), 4396–4404.
(48) Aoneng, C.; Zhen, L.; Saisai, C.; Minghong, W.; Zhangmei, Y.; Zhengwei, C.; Yanli, C.; Shufeng, W.; Qihuang, G.; Yuanfang, L. *Adv. Mater.* **2010**, *22* (1), 103–106.
(49) Chen, X. G.; He, Y. Q.; Zhang, Q.; Li, L. J.; Hu, D. H.; Yin, T. *J. Mater. Sci.* **2010**, *45* (4), 953–960.
(50) Li, D.; Haneda, H. *Chemosphere* **2003**, *51* (2), 129–137.
(51) Jing, L. Q.; Xu, Z. L.; Sun, X. J.; Shang, J.; Cai, W. M. *Appl. Surf. Sci.* **2001**, *180* (3−4), 308–314.
(52) McLaren, A.; Valdes-Solis, T.; Li, G. Q.; Tsang, S. C. *J. Am. Chem. Soc.* **2009**, *131* (35), 12540–12541.
(53) Ho, W.; Yu, J. C.; Lin, J.; Yu, J.; Li, P. *Langmuir* **2004**, *20* (14), 5865–5869.